

Anomalous dimensions and scalar glueball spectroscopy in AdS/QCD

H. Boschi-Filho, N. R. F. Braga, F. Jugeau, M. A. C. Torres

*Instituto de Física, Universidade Federal do Rio de Janeiro, Caixa Postal 68528,
RJ 21941-972 – Brazil*

*E-mails: boschi@if.ufrj.br, braga@if.ufrj.br,
frederic.jugeau@if.ufrj.br, mtorres@if.ufrj.br*

ABSTRACT: An extended version of the AdS/QCD Soft-Wall model that incorporates QCD-like anomalous contributions to the dimensions of gauge theory operators is proposed. This exploratory approach leads to a relation between scalar glueball masses and beta functions. Using this relation, properties of the glueball mass spectroscopy that emerge from phenomenological beta functions proposed in the literature are investigated. The reverse problem is also considered: starting from a linear Regge trajectory which fits the lattice glueball masses, beta functions with different asymptotic infrared behaviours are found. Remarkably, some of them present a fixed point at finite coupling.

KEYWORDS: gauge/gravity correspondence, AdS/CFT correspondence, QCD phenomenology.

Contents

1. Introduction	1
2. Scalar Glueballs	3
2.1 Lattice results	3
2.2 The anomalous dimension of the scalar glueball operator in QCD	4
2.3 The Soft-Wall model	5
3. Improved Soft-Wall model and glueball masses	6
3.1 Soft-Wall model with QCD-like anomalous dimensions	6
3.2 Glueball spectroscopy from improved Soft-Wall model	7
3.2.1 Beta function with an IR fixed point at finite coupling	8
3.2.2 Beta function with a linear IR asymptotic behavior	11
3.2.3 Beta function with a cubic IR asymptotic behavior	12
4. Phenomenological beta functions from Regge-like glueball spectroscopy	14
4.1 Extreme case	16
4.2 Non-extreme case	18
5. Conclusion	20

1. Introduction

The idea that string theory and non-abelian gauge theories are related has been proposed long ago [1]. More recently, an exact equivalence between string theory in ten dimensions and gauge theories in four dimensions was discovered [2, 3, 4]. This relation holds for string theory in $AdS_5 \times S^5$ spacetime and $SU(N)$ Yang Mills theory with large N , extended $\mathcal{N} = 4$ supersymmetry and conformal invariance. This is an example of the AdS/CFT correspondence which also includes other gauge/string dualities in different geometries and dimensions.

In order to apply the idea of gauge/gravity dualities to describe strong interactions, it is necessary to break the conformal invariance. Presently, an exact dual description of QCD is not known. However, in the recent years, some important QCD properties have been reproduced from phenomenological models based on the

AdS/CFT correspondence. Essentially, these so-called AdS/QCD models consist in modifying the AdS geometry with the purpose of breaking the conformal invariance.

An infrared scale in the gauge theory was associated with a localization in the AdS space in Ref.[5]. This way a physical process with an infrared scale in four dimensions is mapped into a region of the AdS space. Using this idea, the correct high energy scaling of hadronic amplitudes for fixed angle scattering was found. This experimentally observed scaling was reproduced by QCD long before in [6].

Putting forward the idea of Ref.[5] to relate AdS/CFT and QCD, in Ref. [7] the scalar glueball spectroscopy was studied using an AdS slice. The size of the slice is related to Λ_{QCD} . Considering boundary conditions in the AdS slice, normalizable modes for the scalar bulk fields dual to scalar glueballs with a discrete spectrum were found. The approach of using an AdS slice to investigate hadronic properties was then called AdS/QCD Hard-Wall model and applied to other particles (see *e.g.* [8]).

It was then realized that the Regge trajectories that can be obtained from the Hard-Wall model are not linear. Then, another AdS/QCD model was proposed to give linear trajectories, especially for vector mesons. This was done with the introduction of a non-dynamical dilaton background field that plays the role of a smooth cut-off in the AdS spacetime [9]. This is called Soft-Wall model and was also applied to study scalar particle properties [10, 11].

The AdS/CFT correspondence deals (in its weakest version) with a strong Yang-Mills coupling. However, a complete holographic description of QCD should incorporate its infrared slavery as well as asymptotic freedom properties. Regarding the importance of the issue, it is worthwhile to explore dual mechanisms able to implement a non-vanishing beta function in the AdS/QCD framework. In this respect, an interesting string-like approach to holographic QCD appeared in [12, 13] (see also [14] for a review). In these models, (dynamical) dilaton potentials are related to QCD-like beta functions and glueball mass spectra were obtained in agreement with lattice results.

In the AdS/CFT correspondence, the masses of supergravity fields are related to the scaling dimensions of the local gauge-invariant dual operators. This relation is derived from the ultraviolet asymptotic behaviour of the bulk-to-boundary propagators [3, 4]. Since the gauge theory is conformal, the beta function vanishes and the scaling dimensions do not get anomalous contribution keeping their canonical - or classical - dimensions. In AdS/QCD, it is usually assumed that the relation between the masses of the bulk fields and the dimensions of the boundary operators is the same as given by AdS/CFT (for an exception, see *e.g.* [15]).

The exploratory approach we follow in this paper aims especially at improving the phenomenological AdS/QCD Soft-Wall model for the case of scalar glueballs. The motivation is that this model predicts masses systematically smaller than lattice results [10]. We will explore the effects on the masses due to the full dimension of the glueball operator. The anomalous contribution implies a modification of the mass of

the dual 5d supergravity field which, in turn, gives rise to a modification of the 4d mass spectrum of the scalar glueballs. We will consider some possible QCD-like beta functions with different infrared behaviours and investigate the main features of the corresponding glueball mass spectra.

The paper is organized as follows: in section 2, we review lattice results, discuss the Soft-Wall model and calculate the anomalous dimension of the scalar glueball operator. In section 3, we study the scalar glueball mass spectrum from three different beta functions considered in the literature. Section 4 is devoted to constructing beta functions able to reproduce linear Regge trajectories of lattice glueball masses.

2. Scalar Glueballs

2.1 Lattice results

The glueball mass spectrum has been the subject of numerous studies in lattice QCD [16, 17, 18, 19], which have provided estimates for the ground-state and a few excited states as shown in Table 1 (for general reviews, see for instance [20, 21]).

	Ref. [16]	Ref. [17]	Ref. [18]	Ref. [19]	
J^{PC}	$N_c = 3$	$N_c = 3$, anisotropic lattice		$N_c = 3$	$N_c \rightarrow \infty$
0^{++}	1.475(30)(65)	1.730(50)(80)	1.710(50)(80)	1.58(11)	1.48(07)
0^{+++}	2.755(70)(120)	2.670(180)(130)		2.75(35)	2.83(22)
0^{++++}	3.370(100)(150)				
0^{+****}	3.990(210)(180)				

Table 1: Lattice scalar glueball mass spectra in GeV. The errors are shown in parenthesis and described in the text.

In the second column, we show the results of Ref.[16] computed for pure $SU(3)_c$ lattice gauge theory. The first number in parenthesis is the statistical error stemming from the continuum-limit extrapolation while the second error accounts for the uncertainty in the string tension σ .

In the third and fourth columns of Table 1, we show results from Refs.[17, 18] where anisotropic lattices have been used with different temporal and spatial spacings. The first error comes from the combined uncertainties from the continuum-limit extrapolation and from the anisotropy, the second from the uncertainty in a hadronic length scale playing a role similar to the string tension.

It is worth pointing out that most of the investigations in lattice consider $SU(N_c)$ theories at finite N_c . However, in the AdS/CFT correspondence, the Yang-Mills theory is in the large N_c limit. In order to compare the large- N_c gauge theory to its finite counterpart, Ref.[19] calculated the lightest and the first excited scalar glueball

masses in gauge theories for increasing N_c and it was found a mass difference for the glueballs of about only 5% between the $N_c = 3$ and the large- N_c gauge theories (see also [22]). These results are shown in the last two columns of Table 1 where we used the mean value $\sqrt{\sigma} = 440$ MeV of [16].

Note also that unquenched lattice QCD only provides the ground-state scalar glueball mass, usually suffering from severe computational difficulties (lack of high statistics, coarse lattice spacing, etc) [23]. Finally, let's mention that unsubtracted QCD spectral sum rules in pure Yang-Mills predicts a ground-state mass around 1.5 GeV [24].

2.2 The anomalous dimension of the scalar glueball operator in QCD

Following [25], the full dimension of the scalar glueball operator can be obtained from the trace anomaly of the QCD energy-momentum tensor [26]:

$$T_\mu^\mu = \frac{\beta(\alpha)}{16\pi\alpha^2} Tr G^2 + (1 + \gamma_m(\alpha)) \sum_{n_f} m_{q_f} \bar{q}_f q_f \quad (2.1)$$

where the beta function is defined as usual as

$$\beta(\alpha(\mu)) \equiv \frac{d\alpha(\mu)}{d \ln(\mu)} \quad (2.2)$$

with μ the renormalization scale, $\alpha \equiv g_{YM}^2/4\pi$ and g_{YM} the Yang-Mills coupling constant.

On the other hand, for any operator \mathcal{O} , we have the following scaling behaviour:

$$\Delta_{\mathcal{O}} \mathcal{O} = -\frac{d\mathcal{O}}{d \ln \mu} \quad (2.3)$$

where the full dimension $\Delta_{\mathcal{O}} = \Delta_{class.} + \gamma(\mu)$ is given in terms of the classical dimension $\Delta_{class.}$ and the anomalous dimension $\gamma(\mu)$. In the following, the fermionic contribution on the *r.h.s* of (2.1) will not be considered, since we are interested only in the equation for the operator $Tr G^2$. Thus, by taking into account the scalar glueball operator contribution of the QCD trace anomaly, Eq.(2.3) gives:

$$\begin{aligned} \Delta_{T_\mu^\mu} \left(\frac{\beta(\alpha)}{8\pi\alpha^2} Tr G^2 \right) &= -\frac{d}{d \ln \mu} \left(\frac{\beta(\alpha)}{8\pi\alpha^2} Tr G^2 \right) \\ &= -\left(\beta'(\alpha) - \frac{2}{\alpha} \beta(\alpha) - \Delta_{G^2} \right) \frac{\beta(\alpha)}{8\pi\alpha^2} Tr G^2 \end{aligned} \quad (2.4)$$

where the prime denotes the derivative with respect to α . The trace T_μ^μ scales classically, that means $\Delta_{T_\mu^\mu} = 4$. This finally implies that the scalar glueball operator $Tr G^2$ has the full dimension¹:

$$\Delta_{G^2} = 4 + \beta'(\alpha) - \frac{2}{\alpha} \beta(\alpha) \quad (2.5)$$

¹An analogous derivation gives $\Delta_{\bar{q}q} = 3 + \frac{\beta(\alpha)\gamma'_m(\alpha)}{(1+\gamma_m)} - \gamma_m(\alpha)$ for the scalar quark bilinear operator with $\gamma_m(\mu) \equiv -\frac{d \ln m_q(\mu)}{d \ln \mu}$ the anomalous dimension of the light quark mass.

which, in terms of the 't Hooft coupling $\lambda \equiv N_c g_{YM}^2 = 4\pi N_c \alpha$, reads

$$\Delta_{G^2} = 4 + \beta'(\lambda) - \frac{2}{\lambda}\beta(\lambda) \quad (2.6)$$

where a prime now denotes a derivative with respect to λ and

$$\beta(\lambda(\mu)) = \frac{d\lambda(\mu)}{d\ln(\mu)}. \quad (2.7)$$

2.3 The Soft-Wall model

In the Soft-Wall model [9], the dynamics of a massive scalar bulk field $X = X(x, z)$ is governed by the following action [10]:

$$S = -\frac{1}{k} \int d^5x \sqrt{-g} e^{-\Phi(z)} [g^{MN} \partial_M X \partial_N X + m_{AdS}^2 X^2] \quad (2.8)$$

where g is the determinant of the metric tensor of AdS_5 given by

$$ds^2 \equiv g_{MN} dx^M dx^N = \frac{R^2}{z^2} (\eta_{\mu\nu} dx^\mu dx^\nu + dz^2), \quad (2.9)$$

with $\eta_{\mu\nu} = \text{diag}(-1, +1, +1, +1)$ the Minkowski $4d$ metric. R is the AdS_5 radius and z is the holographic coordinate allowed to run from zero to infinity. In the following, we will set $R = k = 1$ as they do not enter expressions for the $4d$ particle masses.

The conformal symmetry is smoothly broken by an infrared cut-off represented by a non-dynamical scalar field (the so-called ‘‘background dilaton field’’) chosen as $\Phi(z) = cz^2$ where the parameter c has the dimension of a squared mass. At odds with the Hard-Wall model, this conformal symmetry breaking mechanism allows for linear Regge trajectories. The background field $\Phi(z)$ of the phenomenological Soft-Wall model is not dual to any mode living on the four dimensional boundary spacetime and does not follow from the solution of Einstein equations [27, 28].

The equation of motion for the bulk field $X(x, z)$ is:

$$\partial_z \left(\frac{1}{z^3} e^{-\Phi(z)} \partial_z X \right) + \frac{1}{z^3} e^{-\Phi(z)} \eta^{\mu\nu} \partial_\mu \partial_\nu X - \frac{1}{z^5} e^{-\Phi(z)} m_{AdS}^2 X = 0. \quad (2.10)$$

Representing the scalar field through a $4d$ Fourier transform $\tilde{X}(q, z)$, one finally gets, under the change of function $\tilde{X} = e^{B/2} \tilde{Y}$ with $B(z) = \Phi(z) + 3 \ln(z)$, a $1d$ Schrödinger-like equation:

$$-\partial_z^2 \tilde{Y} + V(z) \tilde{Y} = -q^2 \tilde{Y} \quad (2.11)$$

with the $5d$ effective potential:

$$V(z) = \frac{B'^2}{4} - \frac{B''}{2} + \frac{m_{AdS}^2}{z^2} = c^2 z^2 + \frac{15}{4z^2} + 2c + \frac{m_{AdS}^2}{z^2}. \quad (2.12)$$

The normalizable solutions of Eq.(2.11) correspond to a discrete spectrum of $4d$ masses $q_n^2 \equiv -m_n^2$.

In the Soft-Wall model, one assumes that the $5d$ mass m_{AdS} is related to the scaling dimension of the dual $4d$ boundary operator as given by the AdS/CFT correspondence. For the scalar case, one has:

$$m_{AdS}^2 = \Delta(\Delta - 4). \quad (2.13)$$

Within this holographic set-up, the scalar glueball has been investigated. It is associated with the local gauge-invariant QCD operator $Tr G^2$ defined on the boundary spacetime and which has classical dimension $\Delta_{class.} = 4$. Using (2.13), the bulk mass vanishes:

$$m_{AdS} = 0 \quad (2.14)$$

and the corresponding scalar glueball mass spectrum was found in [10]:

$$m_{G_n}^2 = 4c(n + 2). \quad (2.15)$$

If one fixes c by the mass spectrum of the vector ρ mesons in AdS/QCD [9] as

$$c = 0.2325 \text{ GeV}^2 = (0.482 \text{ GeV})^2, \quad (2.16)$$

one obtains the results shown in Table 2.

0^{++}	0^{+++}	0^{++++}	0^{+++++}
1.364	1.670	1.929	2.156

Table 2: Scalar glueball masses in GeV from the Soft-Wall model [10].

One can see that these results from the Soft-Wall model are systematically smaller² than the lattice values of glueball masses reviewed in subsection **2.1**. Furthermore, it is interesting to note that even changing the value of c , one can not fit the lattice glueball masses using the relations (2.14) and (2.15). In the following, we will see how these masses can be increased by the introduction of the anomalous contribution to the dimension of the scalar glueball operator.

3. Improved Soft-Wall model and glueball masses

3.1 Soft-Wall model with QCD-like anomalous dimensions

Our investigation relies on the Soft-Wall model reviewed in subsection **2.3** from which assumptions and results are well understood. In this paper, considering the case of

²With a negative dilaton parameter and keeping the value (2.16), one gets even smaller masses $m_{G_n}^2 = 4|c|(n + 1)$ [29].

the scalar glueball operator, we will study the main effects on the spectroscopy due to the anomalous contribution of the operator dimension. The anomalous dimension stems from quantum effects and depends on a renormalization scale μ . Since standard AdS/CFT holography implies that the fifth z coordinate is inversely proportional to the $4d$ energy scale μ [30], the full dimension (2.6) and thus the bulk mass (2.13) also depend on the holographic z coordinate.

At small z , any asymptotically AdS spacetime bulk gravity theory satisfies the AdS/CFT relation (2.13) exactly. In the Soft-Wall model, one extrapolates this relation to the large z region, assuming its validity at any energy scale. As a result we write the Eq. (2.13) with the dimension Δ as a function of z :

$$m_{AdS}^2(z) = \Delta(z)(\Delta(z) - 4) \quad (3.1)$$

where the full dimension of the scalar glueball operator $\Delta(z)$ is given by the QCD result (2.6). Note that this procedure has also been followed in the context of finite temperature QCD [25]: considering the conformal AdS/CFT relation (2.13) extended to the case of non-zero anomalous dimensions, the authors approximately reproduced the 2+1 favour lattice QCD estimate of the squared speed of sound as function of the temperature.

Finally, the z -dependent bulk mass generalizes the $5d$ Soft-Wall potential (2.12) to

$$V(z) = c^2 z^2 + \frac{15}{4z^2} + 2c + \frac{1}{z^2} \left[4 + \beta'(\lambda) - \frac{2}{\lambda} \beta(\lambda) \right] \left[\beta'(\lambda) - \frac{2}{\lambda} \beta(\lambda) \right]. \quad (3.2)$$

We will solve the $1d$ -Schrödinger-like equation (2.11) with this effective potential for different phenomenological beta functions and examine the properties of the corresponding glueball mass spectra.

3.2 Glueball spectroscopy from improved Soft-Wall model

In this section, we consider some possible beta functions discussed in the literature [31, 32, 33] and adjust their parameters in order to obtain a mass spectrum compatible with the glueball lattice results. We also demand that the beta functions have an ultraviolet perturbative behaviour similar to QCD for small λ in 1-loop approximation:

$$\beta(\lambda) \sim -b_0 \lambda^2 \quad (3.3)$$

where b_0 is the universal coefficient of the perturbative QCD beta function at leading order:

$$b_0 = \frac{1}{8\pi^2} \left(\frac{11}{3} - \frac{2}{9} n_f \right) \quad (3.4)$$

where we will take $n_f = 0$ such that $b_0 = 11/24\pi^2$. Our analysis deals indeed with the lattice study [16] which was able to predict the four lowest-lying scalar glueball masses in pure $SU(3)_c$.

As a first example of beta function, note that the *r.h.s.* of (3.3) was considered in [31] when investigating the heavy quark-antiquark interaction potential in some Renormalization Group revised AdS/QCD models. However, in our framework, such a beta function cannot give additional anomalous contribution to the effective potential, since the last term in (3.2) vanishes identically in this case.

In the Soft-Wall model of QCD, the fifth coordinate z of the AdS spacetime is identified with μ^{-1} where μ is the renormalization group scale (see, *e.g.* [9, 10, 11, 27] and references therein). Hence, the equation for the beta function becomes in terms of z :

$$\mu \frac{d\lambda(\mu)}{d\mu} = \beta(\lambda(\mu)) \quad \Rightarrow \quad z \frac{d\lambda(z)}{dz} = -\beta(\lambda(z)) \quad (3.5)$$

where the integration constant will be fixed such that $\lambda(z_0) \equiv \lambda_0$ at a particular energy scale z_0 .

3.2.1 Beta function with an IR fixed point at finite coupling

First, let us consider the following beta function [32]:

$$\beta(\lambda) = -b_0 \lambda^2 \left(1 - \frac{\lambda}{\lambda_*} \right) \quad (\lambda_* > 0). \quad (3.6)$$

This beta function vanishes at the infrared fixed point $\lambda = \lambda_*$, reproduces the perturbative $\beta(\lambda) \sim -b_0 \lambda^2$ at 1-loop order in the ultraviolet and behaves as $\beta(\lambda) \sim +\lambda^3$ at large coupling.

The Renormalization Group equation (3.5) for this beta function can be exactly solved, finding:

$$\lambda(z) = \frac{\lambda_*}{1 + W \left(\left(\frac{z_0}{z} \right)^{b_0 \lambda_*} \left(\frac{\lambda_* - \lambda_0}{\lambda_0} \right) e^{\frac{\lambda_* - \lambda_0}{\lambda_0}} \right)} \quad (3.7)$$

which leads to the proper QCD asymptotic behaviour at short distances when z is close to the boundary:

$$\lambda(z) \sim -1/(b_0 \ln z). \quad (3.8)$$

$W(x)$ is the Lambert function and $\lambda(z_0) = \lambda_0$ fixes the integration constant. Then, the $5d$ effective potential (3.2) takes the form:

$$V(z) = c^2 z^2 + \frac{15}{4z^2} + 2c + \frac{b_0 \lambda_*}{z^2} \frac{\left[4 \left(1 + W \left(\left(\frac{z_0}{z} \right)^{b_0 \lambda_*} \left(\frac{\lambda_* - \lambda_0}{\lambda_0} \right) e^{\frac{\lambda_* - \lambda_0}{\lambda_0}} \right) \right)^2 + b_0 \lambda_* \right]}{\left[1 + W \left(\left(\frac{z_0}{z} \right)^{b_0 \lambda_*} \left(\frac{\lambda_* - \lambda_0}{\lambda_0} \right) e^{\frac{\lambda_* - \lambda_0}{\lambda_0}} \right) \right]^4} \quad (3.9)$$

which behaves in the *infrared* as

$$V(z) \sim c^2 z^2 + \frac{[15 + 4b_0 \lambda_* (4 + b_0 \lambda_*)]}{4z^2} + 2c. \quad (3.10)$$

In other words, in the large z limit (when λ goes to λ_*), the contribution to the potential stemming from the anomalous dimension is subleading with respect to the oscillator-like term $c^2 z^2$ coming from the background dilaton field. As a result, the Regge-like behaviour of the Soft-Wall mass spectrum $m_n^2 \sim n$ is preserved for large enough n . Similarly, in the ultraviolet, the anomalous contribution to the potential gives a subleading term with respect to the usual AdS_5 term in $1/z^2$:

$$V(z) \sim c^2 z^2 + \frac{15}{4z^2} + 2c + \frac{4}{b_0 \lambda_*} \frac{1}{z^2 \ln(\frac{z}{z_0})}, \quad (3.11)$$

consistent with the asymptotically conformal behaviour of the gauge theory. Thus, the anomalous contribution in (3.2) consists, for the beta function (3.6), in modifying the $5d$ potential for intermediate values of z only and provides, as it will be shown below, a way of solving the issue discussed at the end of subsection 2.3.

In order to do the numerical analysis, we employ a standard shooting method and choose, as a reference point, $z_0 = 1 \text{ GeV}^{-1}$. Then, substituting $\lambda(z)$ into the beta function and afterwards in the potential (3.2), we solve numerically the corresponding $1d$ -Schrödinger-like equation to find the first four glueball masses which depends on three parameters c , λ_* and λ_0 .

For the isotropic lattice results [16] we are interested in, the best set of parameters able to fit reasonably well the first four masses is $c = -0.36 \text{ GeV}^2$, $\lambda_* = 350$ and $\lambda_0 = 18.5$. The corresponding masses are shown in Table 3 while the effective potentials for the minimal and the improved Soft-Wall models are displayed in Figure 1.

c	λ_0	λ_*	0^{++}	0^{++*}	0^{+++}	0^{++++}
-0.36	18.5	350	1.497	2.307	3.056	3.625

Table 3: Scalar glueball masses from the phenomenological beta function with an IR fixed point at finite coupling (3.6). Masses and c are expressed in GeV and GeV^2 respectively. λ_0 and λ_* are dimensionless.

While the masses of the first and second excited states are a bit too small, being slightly outside the error bars, the first and the fourth masses lie within the range of values allowed by [16]. Our fit consistently predicts a coupling λ_0 at the scale $z_0 = 1 \text{ GeV}^{-1}$ which is bigger³ than the world average (WA) value of the strong coupling [34]:

$$\alpha_s = 0.1184 \Rightarrow \lambda_0^{(WA)} = 4.464 \quad (N_c = 3), \quad (3.12)$$

corresponding to the Z^0 boson mass

$$z_0 \equiv 1/M_{Z^0} = 0.010966 \text{ GeV}^{-1}. \quad (3.13)$$

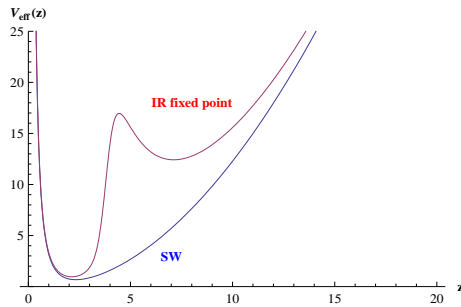


Figure 1: The effective potentials from the minimal (2.12) and improved (3.2) Soft-Wall models with the IR fixed point beta function (3.6). The values of the parameters are those listed in Table 3.

Interestingly, c turns out to be negative with an absolute value about twice larger than the dilaton parameter $c = 0.2325 \text{ GeV}^2$ (2.16) evaluated in the Soft-Wall model from the ρ meson mass. A negative dilaton parameter has been introduced in the Soft-Wall models of QCD in [35] and remains a subject of debate (see, *e.g.* [29, 36]). On the other hand, a positive c gives rise to a less satisfactory spectrum, most of the masses being outside their uncertainty intervals. A reason for that can be seen in Eq.(3.2) where a positive c increases the minimum of the effective potential.

As the first two excited states appears a bit too small, one could try to slightly vary the parameters. Letting the two other parameters λ_* and λ_0 unchanged, to increase c obviously makes the potential steeper in the infrared and increases indeed the masses. Then, it appears a lower bound for c around $-(0.47) \text{ GeV}^2$ for which the ground-state mass reaches the upper bound allowed by [16]. Nevertheless, the rest of the spectrum grows too slowly: while the second excited state becomes close to its lower bound (3.112 GeV compared with 3.120 GeV), the first excited state remains too small (2.369 GeV compared with 2.565 GeV). The fourth mass still remains within its uncertainty range. The same mechanism occurs if we decide instead to increase λ_0 with the upper bound $\lambda_0 = 19.4$. Finally, increasing λ_* raises the peak shown in Figure 1 for intermediate z without modifying its location. As a result, the potential takes for the lowest-lying states the shape of a well potential: for λ_* large enough, their masses become invariant and reach for the first three masses 1.502, 2.388 and 3.238 GeV respectively, the first excited state being as usual too light. A reason for this general fact is the important gap between the ground-state and the first excited state [16] (around 1.3 GeV, to be compared, for instance, with the smaller gap of 0.94 GeV for anisotropic lattice [17]).

³Note that the WA estimate was obtained from many various processes involving quark flavours (τ and heavy quarkonia decays, lattice QCD, deep inelastic scattering, etc).

3.2.2 Beta function with a linear IR asymptotic behavior

The model beta function [31, 33]:

$$\beta(\lambda) = -\frac{b_0\lambda^2}{1+b_1\lambda} \quad (b_0, b_1 > 0) \quad (3.14)$$

behaves like the perturbative QCD beta function at 1-loop order and decreases asymptotically as $-\lambda$ in the infrared. Solving (3.5) for this beta function, we find:

$$\lambda(z) = \frac{1}{b_1 W\left(\frac{e^{\frac{1}{b_1\lambda_0}}}{b_1\lambda_0} \left(\frac{z_0}{z}\right)^{b_0/b_1}\right)}. \quad (3.15)$$

Then, the $5d$ potential reads as

$$V(z) = c^2 z^2 + \frac{15}{4z^2} + 2c + \frac{1}{z^2} \frac{b_0}{b_1} \frac{\left[4 \left(1 + W\left(\frac{e^{\frac{1}{b_1\lambda_0}}}{b_1\lambda_0} \left(\frac{z_0}{z}\right)^{b_0/b_1}\right)\right)^2 + \frac{b_0}{b_1}\right]}{\left[1 + W\left(\frac{e^{\frac{1}{b_1\lambda_0}}}{b_1\lambda_0} \left(\frac{z_0}{z}\right)^{b_0/b_1}\right)\right]^4} \quad (3.16)$$

which presents the same subleading infrared and ultraviolet asymptotic behaviours than the beta function (3.6) considered before. Thus, the AdS effective potential gets modifications only for intermediate z . In particular, the squared masses m_n^2 still follows a linear Regge trajectory for large n . Figure 2 shows the effective potentials for the values of parameters listed in Table 4.

With the beta function (3.14), the masses depend on the parameters c , b_1 and λ_0 . The result of the fit of the first four masses is shown in Table 4 and corresponds to the set of parameters $c = -0.25 \text{ GeV}^2$, $b_1 = 1.2 \times 10^{-3}$ and $\lambda_0 = 19$. In this case, only the first excited state cannot be fitted within the error bars, being slightly too small. Also in this case, the dilaton parameter is negative and, furthermore, very close in absolute value to the minimal Soft-Wall estimate (2.16). The coupling λ_0 we figured out, fitted at the energy scale $z_0 = 1 \text{ GeV}^{-1}$, is quite close to the λ_0 we found in the case of the IR fixed point beta function (19 compared with 18.5), showing consistency in our results.

c	b_1	λ_0	0^{++}	0^{++*}	0^{+++}	0^{++++}
-0.25	1.2×10^{-3}	19	1.484	2.434	3.346	4.239

Table 4: Glueball masses in GeV for the the beta function (3.14). c is expressed in GeV^2 while b_1 and λ_0 are dimensionless.

Changing one parameter while keeping fixed the other two allows one to see that, on the one hand, c and λ_0 are bounded by the same limit values as derived for the IR fixed point beta function. On the other hand, the parameter b_1 plays the same

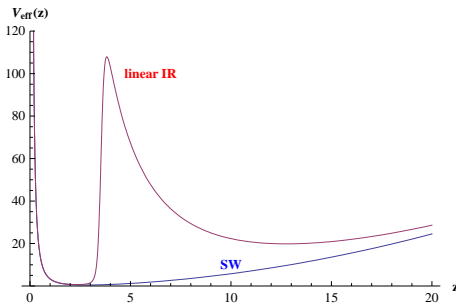


Figure 2: The effective potentials from the minimal (2.12) and improved (3.2) Soft-Wall models with the linear IR beta function (3.14). The values of the parameters are listed in Table 3.

role than the fixed point λ_* such that, for b_1 large enough, the lowest-lying masses become independent of b_1 ⁴.

From our analysis, it thus appears that the model beta function (3.14) seems favoured with respect to the previous case (3.6). Indeed, the former allows one to fit the first four masses reasonably well with the exception only of the first excited state whose the gap with the ground-state might be, as discussed at the end of subsection 3.2.1, too high regarding other studies [17].

3.2.3 Beta function with a cubic IR asymptotic behavior

We consider now the following beta function [31]:

$$\beta(\lambda) = -b_0\lambda^2 - b_1\lambda^3 \quad (b_0, b_1 > 0) \quad (3.17)$$

which behaves as $-\lambda^3$ in the infrared.

The solution of the Renormalization Group equation reads

$$\lambda(z) = -\frac{b_0}{b_1} \frac{1}{1 + W_{-1} \left(-\left(\frac{z}{z_0}\right)^{\frac{b_0^2}{b_1}} \left(1 + \frac{b_0}{b_1\lambda_0}\right) e^{-(1+\frac{b_0}{b_1\lambda_0})} \right)} \quad (3.18)$$

imposing $\lambda(z_0) = \lambda_0$. $W_{-1}(x)$ is the generalized Lambert function of order -1 which leads, on the one hand, to the QCD-like perturbative behaviour (3.8) at small coupling. On the other hand, because of the analytical properties of $W_{-1}(x)$, the coupling λ becomes infinite for a finite value of z given by

$$z_{max} = \frac{z_0 e^{\frac{1}{b_0\lambda_0}}}{\left(1 + \frac{b_0}{b_1\lambda_0}\right)^{b_1/b_0^2}}. \quad (3.19)$$

⁴While b_1 in (3.14) has nothing to do with $b_1^{(pert)}$ of the perturbative QCD beta function, let's remark that they seem numerically close ($b_1^{(pert)} \approx 0.9 \times 10^{-3}$ for $n_f = 0$). Nevertheless, the shape of the 5d potential displayed in Figure 2 is very sensitive to the value of b_1 .

In other words, the implementation of the beta function (3.17) into the Soft-Wall framework gives rise to an AdS slice $0 < z < z_{max}$. In contrast with the Soft-Wall model, the 5d potential (3.2)

$$V(z) = c^2 z^2 + \frac{15}{4z^2} + 2c - \frac{1}{z^2} b_1 \lambda(z)^2 (4 - b_1 \lambda(z)^2) \quad (3.20)$$

goes to infinity at $z = z_{max}$: unexpectedly, there is the formation of a hard wall located at z_{max} (independent of c) and the solutions of the Schrödinger-like equation (2.11) will be non-vanishing only in the region $0 < z < z_{max}$.

The fact that the background was initially of the Soft-Wall model does not have significant influence in getting the glueball mass spectrum in this case, as shown in Table 5 and Figure 3 where a positive as well as negative dilaton parameter c is in fact an acceptable value. Furthermore, the 5d potential having the shape of a sharp well, the Regge-like behaviour of the squared masses is lost and we have instead $m_n^2 \sim n^2$ for large n .

c	b_1	λ_0	z_{max}	0^{++}	0^{++*}	0^{+++}	0^{+++*}
-0.3	10^{-9}	17.9	3.330	1.476	2.480	3.453	4.415
0.05	1.3×10^{-5}	17	3.436	1.522	2.465	3.393	4.315

Table 5: Masses for the scalar glueball ground-state and the radial excitations $J^{PC} = 0^{++}$ for the phenomenological beta function (3.17) with a cubic IR asymptotic behavior. Masses are expressed in GeV, c in GeV^2 and b_1 is dimensionless. For completeness, we also show the values of z_{max} expressed in GeV^{-1} .

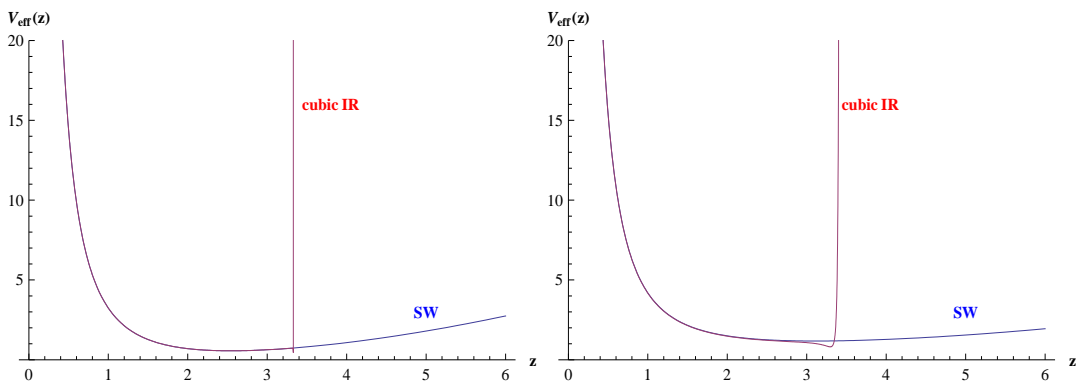


Figure 3: The effective potentials from the minimal and improved Soft-Wall models with the cubic IR beta function (3.17) for c negative (left panel) and c positive (right panel). The values of the parameters are listed in Table 5.

Both for a positive and a negative dilaton parameter, the first excited state is slightly too light although the result seems a bit better than for the IR linear

and the IR fixed point beta functions considered in the subsection **3.2.1** and **3.2.2**. Nevertheless, the fourth mass is either too large (for c negative) or approaches closely its upper bound (for c positive). This result was expected since the masses of the higher states are significantly increased by the presence of the hard wall.

4. Phenomenological beta functions from Regge-like glueball spectroscopy

The glueball masses obtained from lattice studies shown in Table 1 lie approximately in linear Regge trajectories, namely, the square of the masses has approximately a linear relation with the radial quantum number. In this section, we build up beta functions that reproduce this behaviour. In particular, we will consider the four masses from the isotropic lattice calculations shown in the second column of Table 1. A linear Regge trajectory which fits these masses corresponds to

$$m_n^2 = 4.50n + 2.51, \quad (4.1)$$

where the squared masses are given in GeV^2 . This Regge trajectory implies the glueball masses given in Table 6. The first mass is just 1% above the lattice result including the error bar. The other three masses are within the error bars.

0^{++}	0^{+++}	0^{++++}	0^{+++++}
1.585	2.648	3.393	4.001

Table 6: Glueball masses in GeV from the Regge trajectory of Eq.(4.1).

In order to obtain the classes of beta functions that lead to this Regge linear spectrum, we consider the Soft-Wall potential modified by the contribution from the anomalous dimension of the scalar glueball operator (3.2):

$$V(z) = c^2 z^2 + \frac{15}{4z^2} + 2c + \frac{1}{z^2} [4 + f(z)] f(z) \quad (4.2)$$

where

$$f(z) \equiv \frac{d\beta(\lambda)}{d\lambda} - \frac{2}{\lambda}\beta(\lambda). \quad (4.3)$$

It is convenient to rewrite $f(z)$ in terms of the coupling $\lambda(z)$:

$$\begin{aligned} f(z) &= -1 - z \left(\frac{\lambda''}{\lambda'} - 2 \frac{\lambda'}{\lambda} \right) \\ &= -1 - z \frac{d}{dz} \left(\ln \frac{\lambda'}{\lambda^2} \right) \end{aligned} \quad (4.4)$$

where a prime denotes a derivative with respect to z .

We use the following ansatz:

$$(f(z) + 2)^2 = k + k_1 z^2 + k_2 z^4, \quad (4.5)$$

with k , k_1 and k_2 constants, that will be fixed in terms of c , as we show in the sequence. The positivity of this ansatz requires:

$$k_1^2 \leq 4kk_2. \quad (4.6)$$

From the Eqs.(4.4) and (4.5), we have thus to solve the differential equation:

$$\frac{d}{dz} \ln \left(\frac{\lambda'(z)}{\lambda^2(z)} \right) = \frac{1}{z} \mp \frac{1}{z} \sqrt{k + k_1 z^2 + k_2 z^4}. \quad (4.7)$$

To reproduce the QCD asymptotic behaviour at leading order shown in Eq.(3.8), we impose that

$$\lim_{z \rightarrow 0} \left(\frac{1}{\lambda(z)} \right)' = -\frac{b_0}{z}, \quad (4.8)$$

which, in turn, implies:

$$\lim_{z \rightarrow 0} \frac{d}{dz} \ln \left(\frac{\lambda'(z)}{\lambda^2(z)} \right) = -\frac{1}{z}. \quad (4.9)$$

Hence, we must have $k = 4$. For small z , we also must take the upper sign in Eq.(4.7). Note that this analysis of the perturbative small z limit does not impose the sign of Eq.(4.7) for large values of z as it will be discussed below.

Then, the potential takes the form:

$$V(z) = (c^2 + k_2) z^2 + \frac{15}{4z^2} + (2c + k_1). \quad (4.10)$$

Solving the 1d-Schrödinger-like equation (2.11) with this potential, one finds the following 4d mass spectrum:

$$m_n^2 = 4\sqrt{c^2 + k_2} n + 6\sqrt{c^2 + k_2} + 2c + k_1. \quad (4.11)$$

This equation is matched to the glueball linear Regge trajectory of Eq.(4.1) yielding:

$$\begin{cases} k_1(c) = -\frac{106}{25} - 2c, \\ k_2(c) = \frac{81}{64} - c^2. \end{cases} \quad (4.12)$$

With the positivity condition (4.6), the allowed range of the remaining parameter c is $c_{min} \leq c \leq c_{max}$ with

$$c_{min} = -(0.983 \text{ GeV})^2 \quad \text{and} \quad c_{max} = (0.344 \text{ GeV})^2. \quad (4.13)$$

The extreme values of the dilaton parameter saturate the positivity condition, *i.e.*, $k_1^2 = 16k_2$. Also here, we observe the possibility of negative values for c and the fact

that the allowed range of negative values is almost ten times larger than the allowed range for positive values of c . We also note that k_1 , expressed in terms of c , can only be negative.

Let us now determine the corresponding beta functions. They will depend on the two parameters c and λ_0 . We will treat separately the cases $k_1^2 = 16k_2$ (extreme case) and $k_1^2 < 16k_2$ (non-extreme case) since then the differential equation (4.7) assumes different forms.

4.1 Extreme case

In this case, c is fixed and can take the two values c_{min} and c_{max} , corresponding to $k_1 = -2.307$ and $k_1 = -4.477$ respectively. Then, Eq.(4.7) reduces to:

$$1 - z \frac{d}{dz} \left(\ln \frac{\lambda'}{\lambda^2} \right) = \pm \left(2 + \frac{k_1}{4} z^2 \right). \quad (4.14)$$

Since k_1 is negative, there is a critical value of z given by $z_c^2 = -8/k_1$. We get $z_c = 1.862 \text{ GeV}^{-1}$ and $z_c = 1.337 \text{ GeV}^{-1}$ for $c = c_{min}$ and $c = c_{max}$ respectively. For $z < z_c$, the sign of Eq.(4.14) is fixed by the perturbative limit. For $z \geq z_c$, we are free to choose the sign without spoiling the smoothness of the coupling $\lambda(z)$. In the following, we are going to consider the two possibilities.

- First, we take the upper sign of Eq.(4.14) for all values of z and find an analytical solution:

$$\lambda(z) = \frac{\lambda_0}{1 - b_0 \frac{\lambda_0}{2} \left[Ei\left(-\frac{k_1}{8} z^2\right) - Ei\left(-\frac{k_1}{8} z_0^2\right) \right]}, \quad (4.15)$$

expressed in terms of the exponential integral function $Ei(x)$. Furthermore, we will choose to fix the remaining parameter $\lambda(z_0) = \lambda_0$ at the energy scale $z_0 = 1/M_{Z^0}$ given by (3.13) and which corresponds to the world average value of the 't Hooft coupling $\lambda^{(WA)} = 4.464$ (3.12). While λ_0 with $n_f = 0$ is not equal to $\lambda^{(WA)}$, it is not very different in the perturbative regime. By slightly varying λ_0 around its WA value in Eq.(4.15), we will observe no strong effect in the behaviour of the coupling constant. On the contrary, we will see in the subsection 4.2 when c is not extreme that a small variation of λ_0 can drastically change the low energy behaviour of the coupling.

The beta function reads

$$\beta(z) \equiv -z\lambda'(z) = - \frac{\lambda_0^2 b_0 e^{-\frac{k_1}{8} z^2}}{\left\{ 1 - b_0 \frac{\lambda_0}{2} \left[Ei\left(-\frac{k_1}{8} z^2\right) - Ei\left(-\frac{k_1}{8} z_0^2\right) \right] \right\}^2}. \quad (4.16)$$

Considering the two possible values for c which fixes k_1 and k_2 , we have plotted in Figure 4 the couplings and the beta functions in terms of the holographic coordinate z for four values of λ_0 around $\lambda^{(WA)}$. Both $\lambda(z)$ and $\beta(z)$ diverge at a finite value of

$z = z_{max}$ where the denominators in the Eqs.(4.15) and (4.16) vanish. z_{max} depends on λ_0 and is larger for c_{min} than for c_{max} . In Figure 5, we show the dependence of the beta functions on the coupling λ for the two extreme values of c .

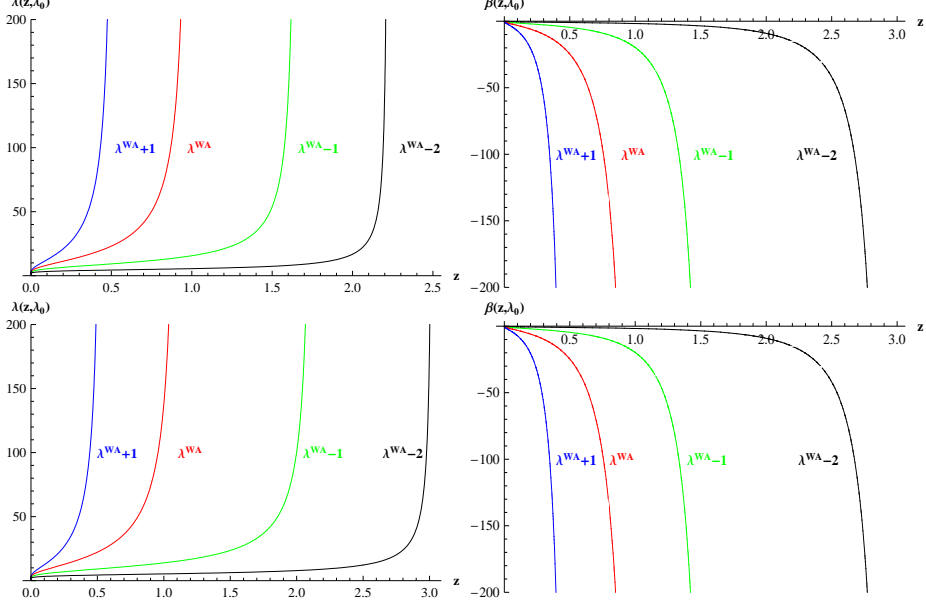


Figure 4: The 't Hooft couplings $\lambda(z)$ and the phenomenological beta functions $\beta(z)$ as defined in (4.15) and (4.16) for different values of λ_0 close to $\lambda_0^{(WA)}$ and $c = c_{max}$ (upper panels) and $c = c_{min}$ (lower panels).

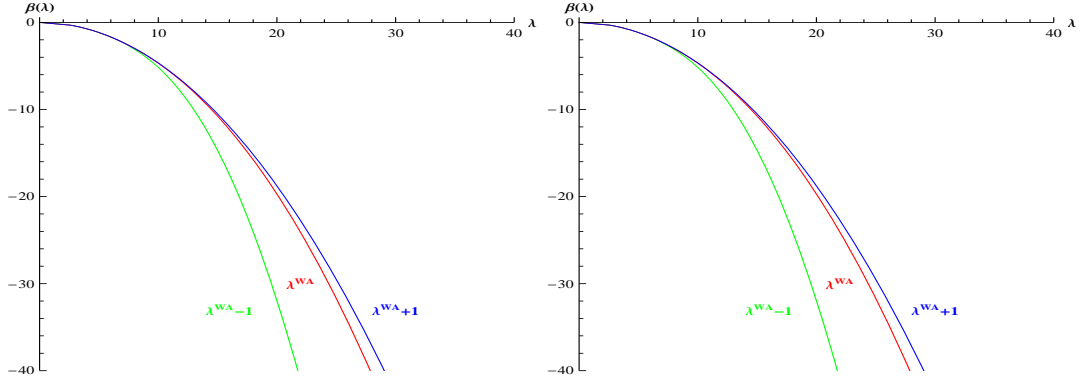


Figure 5: The phenomenological beta functions (4.16) in terms of λ for different values of λ_0 close to $\lambda_0^{(WA)}$ when $c = c_{max}$ (left panel) and $c = c_{min}$ (right panel).

- Secondly, when we choose for the Eq.(4.14) the following form:

$$z \frac{d}{dz} \left(\ln \frac{\lambda'}{\lambda^2} \right) = \begin{cases} -(1 + \frac{k_1}{4} z^2) & z < z_c, \\ (3 + \frac{k_1 z^2}{4}) & z \geq z_c, \end{cases} \quad (4.17)$$

with a change of sign at z_c , we observe that the shapes of the 't Hooft coupling and of the beta function are similar to the previous case, shown in Figure 4, and diverge at $z = z_{max}$.

Depending on λ_0 , z_{max} can be smaller or larger than z_c . Note that decreasing λ_0 increases z_{max} . When $z_{max} < z_c$, only the solution (4.15) is present. This happens when $\lambda_0 = 3.942$ (negative c) and $\lambda_0 = 3.712$ (positive c). When $z_{max} > z_c$, we have another solution, given by the complete solution of Eq.(4.17):

$$\lambda(z) = (1 - \Theta(z - z_c)) \lambda_{<}(z) + \frac{\Theta(z - z_c)}{\frac{1}{\lambda_{<}(z_c)} + \frac{b_0}{2} \left(\frac{z^2}{z_c^2} + 1 \right) e^{2 - \frac{z^2}{z_c^2}} - b_0 e} \quad (4.18)$$

and

$$\beta(z) = (1 - \Theta(z - z_c)) \beta_{<}(z) - \frac{\Theta(z - z_c)}{\left[\frac{1}{\lambda_{<}(z_c)} + \frac{b_0}{2} \left(\frac{z^2}{z_c^2} + 1 \right) e^{2 - \frac{z^2}{z_c^2}} - b_0 e \right]^2} \frac{b_0 z^4}{z_c^4} e^{2 - \frac{z^2}{z_c^2}}. \quad (4.19)$$

where $\Theta(z)$ is the step function and $\lambda_{<}(z)$ and $\beta_{<}(z)$ are given by (4.15) and (4.16).

Let us emphasize that changing the sign in Eq.(4.14) leads to two different solutions. Nevertheless, the data we use do not allow us to select a unique phenomenological beta function.

4.2 Non-extreme case

In this case, the square root on the *r.h.s.* of Eq.(4.7) does not vanish for any value of z . Therefore, the upper sign is the only possibility here. Then, we find out:

$$\left(\frac{1}{\lambda} \right)' = -\frac{b_0}{4z} \frac{\left(\sqrt{4 + k_1 z^2 + k_2 z^4} + \frac{k_1}{4} z^2 + 2 \right) (k_1 + 4\sqrt{k_2})^{\frac{k_1}{4\sqrt{k_2}}}}{\left(2\sqrt{k_2} \sqrt{4 + k_1 z^2 + k_2 z^4} + 2k_2 z^2 + k_1 \right)^{\frac{k_1}{4\sqrt{k_2}}}} e^{1 - \frac{1}{2} \sqrt{4 + k_1 z^2 + k_2 z^4}} \quad (4.20)$$

which cannot be solved analytically. The parameters are λ_0 and c . The latter, calculated from (4.6) and (4.12), can assume any value inside the range $c_{min} < c < c_{max}$ (4.13).

In order to analyse the behaviour of the general equation (4.20), let's write its integral from z to z_0 under the form:

$$\frac{1}{\lambda_0} - \frac{1}{\lambda(z)} = F(z, z_0). \quad (4.21)$$

Then, the 't Hooft coupling reads

$$\lambda(z) = \frac{\lambda_0}{1 - \lambda_0 F(z, z_0)}. \quad (4.22)$$

For large enough values of λ_0 , namely $\lambda_0 > \lambda_0^{(limit)} = 3.234$, there is always a $z = z_{max}$ at which $\lambda(z)$ diverges. Moreover, this occurs for any value of c . Then, the shapes of $\lambda(z)$, $\beta(z)$ and $\beta(\lambda)$ are similar to the ones displayed in Figures 4 and 5.

On the contrary, for $\lambda_0 < \lambda_0^{(limit)}$, the results turn out to be drastically different. In the sequel, we will consider the illustrative case $\lambda_0 = 3.164$. While seemingly totally arbitrary, this choice will allow us to discuss qualitatively all the possible behaviours the coupling and the beta function can take. We could have also chosen any other value for λ_0 , the crucial point being that λ_0 must be smaller than $\lambda_0^{(limit)}$.

First, we observe that for c close to the extreme values of its allowed range, the coupling solution remains singular. Like the two cases considered above, there is a value $z = z_{max}$ for which the denominator $1 - \lambda_0 F(z_{max}, z_0)$ vanishes.

However, there is an interval for c , namely

$$c \in] - (0.860 \text{ GeV})^2, -(0.548 \text{ GeV})^2[\quad (4.23)$$

for which this denominator never vanishes. Note that this interval only contains negative values of c . As a result, the coupling and the beta function are finite for all z . We show in Figure 6 the behaviour of $1 - \lambda_0 F(z, z_0) = \lambda_0/\lambda(z)$ as a function of z and c .

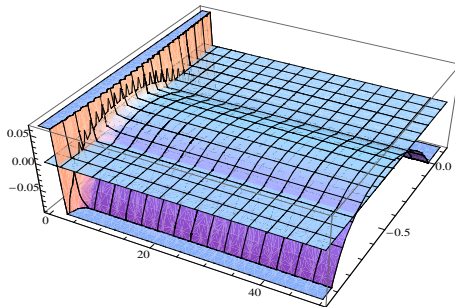


Figure 6: The function $\lambda_0/\lambda(z)$ and the zero-value plane surface. The coordinate z and the parameter c run respectively from 0 to 50 and from its extreme values $c_{min} \simeq -(0.983 \text{ GeV})^2$ to $c_{max} \simeq (0.344 \text{ GeV})^2$.

Further, in Figure 7, we show the 't Hooft couplings and the phenomenological beta functions for some noticeable values of c . The red and green curves correspond to the two limit values $c = -(0.860 \text{ GeV})^2$ and $c = -(0.548 \text{ GeV})^2$ beyond which $\lambda(z)$ and $\beta(z)$ are singular at z_{max} . On the other hand, for any value of the parameter c inside the interval (4.23), the 't Hooft coupling presents an *IR fixed point* λ_* . Accordingly, the beta function *vanishes* for sufficiently large z . Figure 7 displays the case $c = -(0.800 \text{ GeV})^2$ and the mid-value $c = -(0.721 \text{ GeV})^2$ as well.

In Table 7, we list the numerical estimates for z_{max} and λ_* for some characteristic values of c . Note that λ_* takes very different values.

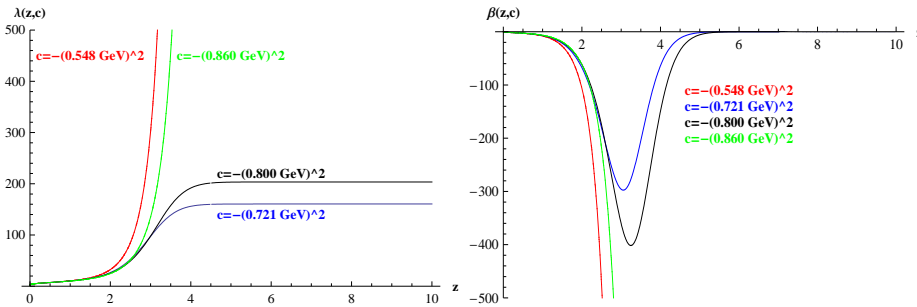


Figure 7: The 't Hooft couplings $\lambda(z, c)$ and the associated beta function $\beta(z, c)$ in terms of z for some remarkable values of c in the case $\lambda_0 < \lambda^{(limit)}$.

c (GeV ²)	z_{max} (GeV)	λ_*
$-(0.548)^2$	4.246	
$-(0.549)^2$		62314
$-(0.721)^2$		161
$-(0.800)^2$		203
$-(0.859)^2$		49819
$-(0.860)^2$	4.496	

Table 7: Numerical estimates for z_{max} and λ_* for some values of the dilaton parameter inside the interval (4.23) and immediately beyond.

Finally, we plot the beta functions in terms of λ in Figure 8. Within the interval (4.23), $\beta(\lambda)$ shows the typical behaviour associated with an IR fixed point at finite coupling. On the other hand, for c close to its extremal values, we recover the monotonous decreasing of $\beta(\lambda)$.

5. Conclusion

The AdS/CFT correspondence provides a well-defined relation between the dimensions of Yang-Mills theory operators and the bulk masses of the corresponding supergravity fields. In the AdS/QCD models, one in general assumes that the same relation holds. Here we have followed this approach. For QCD-like gauge theories, the dimensions of operators receive anomalous contributions coming from quantum effects. In this paper, we have developed an extended AdS/QCD approach taking into account the anomalous dimensions of the operators entering the expression of the QCD trace anomaly. We considered the scalar glueball spectroscopy within the AdS/QCD Soft-Wall framework. Following this extended model, the mass of the scalar bulk field acquires a dependence on the holographic coordinate. This modi-

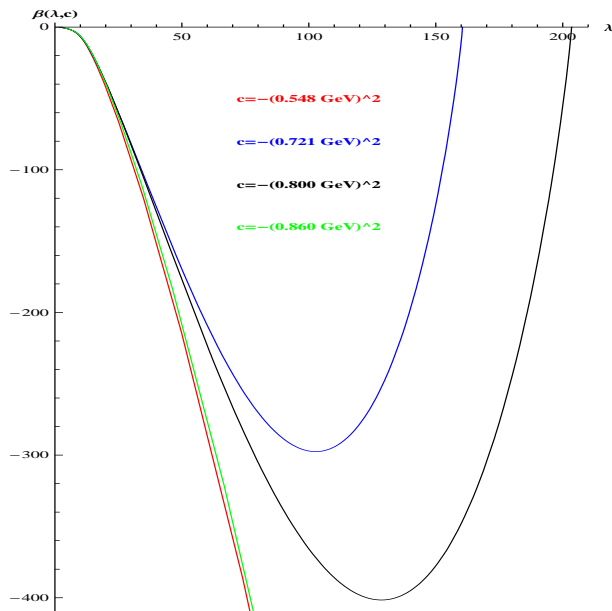


Figure 8: beta functions $\beta(\lambda, c)$ in terms of λ for $\lambda_0 < \lambda^{(limit)}$ and different values of c in the non-extreme case when $k_1^2 < 16k_2$.

fication is then reflected in the eigenvalue equation that determines the $4d$ glueball masses.

In Chapter 3, we considered some possible model QCD beta functions discussed in the literature and calculated the corresponding glueball mass spectra, comparing with the isotropic lattice results. In particular, a beta function with an asymptotic IR cubic behaviour gives rise to the formation of a hard-wall in the $5d$ effective potential.

In Chapter 4, we started from the linear Regge trajectory calculated using glueball lattice results and found out beta functions that lead to this spectrum. We find different types of beta functions classified according to their IR behaviour. For a class of beta functions, an IR cutoff z_{max} , which is not present in the Soft-Wall model, naturally emerges and gives rise to asymptotically decreasing $\beta(\lambda)$. There is also another class of beta functions that vanish at large λ , leading to an IR fixed point at finite coupling. The IR vanishing beta functions offer a large range of possible values for the IR fixed coupling.

A better knowledge of mass spectroscopy in different channels would further constrain the holographic parameters. This could help answering the question of the presence or not of an IR fixed point and its value.

Acknowledgments: The authors are partially supported by Capes and CNPq, Brazilian agencies. One of us, F.J., is grateful to J. A. Helayël-Neto for his hospitality at the CBPF during the completion of this work.

References

- [1] G. 't Hooft, “*A Planar Diagram Theory for Strong Interactions*”, Nucl. Phys. B **72**, 461 (1974).
- [2] J. M. Maldacena, “*The large N limit of superconformal field theories and supergravity*”, Adv. Theor. Math. Phys. **2**, 231 (1998) [Int. J. Theor. Phys. **38**, 1113 (1999)]. [arXiv:hep-th/9711200].
- [3] S. S. Gubser, I. R. Klebanov and A. M. Polyakov, “*Gauge theory correlators from non-critical string theory*”, Phys. Lett. B **428**, 105 (1998). [arXiv:hep-th/9802109].
- [4] E. Witten, “*Anti-de Sitter space and holography*”, Adv. Theor. Math. Phys. **2**, 253 (1998). [arXiv:hep-th/9802150].
- [5] J. Polchinski and M. J. Strassler, “*Hard scattering and gauge/string duality*”, Phys. Rev. Lett. **88**, 031601 (2002) [arXiv:hep-th/0109174].
- [6] V. A. Matveev, R. M. Muradian and A. N. Tavkhelidze, “*Automodellism in the large-angle elastic scattering and structure of hadrons*”, Lett. Nuovo Cim. **7**, 719 (1973). S. J. Brodsky and G. R. Farrar, “*Scaling Laws At Large Transverse Momentum*”, Phys. Rev. Lett. **31**, 1153 (1973), “*Scaling Laws For Large Momentum Transfer Processes*”, Phys. Rev. D **11**, 1309 (1975).
- [7] H. Boschi-Filho and N. R. F. Braga, “*QCD/String holographic mapping and glueball mass spectrum*”, Eur. Phys. J. C **32**, 529 (2004) [arXiv:hep-th/0209080], “*Gauge/string duality and scalar glueball mass ratios*”, JHEP **0305**, 009 (2003) [arXiv:hep-th/0212207].
- [8] G. F. de Teramond & S. J. Brodsky, “*The hadronic spectrum of a holographic dual of QCD*,” Phys. Rev. Lett. **94**, 201601 (2005) [arXiv:hep-th/0501022]. Erlich et al., “*QCD and a holographic model of hadrons*”, Phys. Rev. Lett. **95** (2005) 261602.
- [9] A. Karch, E. Katz, D. T. Son and M. A. Stephanov, “*Linear confinement and AdS/QCD*”, Phys. Rev. D **74**, 015005 (2006) [arXiv:hep-ph/0602229].
- [10] P. Colangelo, F. De Fazio, F. Jugeau and S. Nicotri, “*On the light glueball spectrum in a holographic description of QCD*”, Phys. Lett. B **652**, 73 (2007) [arXiv:hep-ph/0703316], “*Investigating AdS/QCD duality through scalar glueball correlators*”, Int. J. Mod. Phys. **A24** (2009) 4177-4192 [arXiv:hep-ph/0711.4747]. P. Colangelo, F. De Fazio, F. Giannuzzi, F. Jugeau & S. Nicotri, “*Light scalar mesons in the soft-wall model of AdS/QCD*”, Phys. Rev. **D78** (2008) 055009 [arXiv:hep-ph/0807.1054].
- [11] H. Forkel, “*Holographic glueball structure*”, Phys. Rev. **D78** (2008) 025001 [arXiv:hep-ph/0711.1179].
- [12] U. Gursoy and E. Kiritsis, “*Exploring improved holographic theories for QCD: Part I*”, JHEP **0802**, 032 (2008) [arXiv:0707.1324 [hep-th]].

- [13] U. Gursoy, E. Kiritsis and F. Nitti, “*Exploring improved holographic theories for QCD: Part II*”, JHEP **0802**, 019 (2008) [arXiv:0707.1349 [hep-th]].
- [14] U. Gursoy, E. Kiritsis, L. Mazzanti, G. Michalogiorgakis and F. Nitti, “*Improved Holographic QCD*”, Lect. Notes Phys. **828**, 79 (2011) [arXiv:1006.5461 [hep-th]].
- [15] A. Vega and I. Schmidt, *Modes with variable mass as an alternative in AdS/QCD models with chiral symmetry breaking*, Phys. Rev. **D82** (2012) 115023 [arXiv:hep-ph/1005.3000].
- [16] H. B. Meyer, “*Glueball regge trajectories*”, hep-lat/0508002.
- [17] C. J. Morningstar and M. J. Peardon, “*The Glueball spectrum from an anisotropic lattice study*”, Phys. Rev. D **60**, 034509 (1999) [hep-lat/9901004].
- [18] Y. Chen, A. Alexandru, S. J. Dong, T. Draper, I. Horvath, F. X. Lee, K. F. Liu and N. Mathur *et al.*, “*Glueball spectrum and matrix elements on anisotropic lattices*”, Phys. Rev. D **73**, 014516 (2006) [hep-lat/0510074].
- [19] B. Lucini and M. Teper, “*SU(N) gauge theories in four-dimensions: Exploring the approach to $N = \infty$* ”, JHEP **0106**, 050 (2001) [hep-lat/0103027].
- [20] V. Mathieu, N. Kochelev and V. Vento, “*The Physics of Glueballs*”, Int. J. Mod. Phys. E **18**, 1 (2009) [arXiv:0810.4453 [hep-ph]].
- [21] E. Klempt and A. Zaitsev, “*Glueballs, Hybrids, Multiquarks. Experimental facts versus QCD inspired concepts*”, Phys. Rept. **454**, 1 (2007) [arXiv:0708.4016 [hep-ph]].
- [22] B. Lucini, A. Rago and E. Rinaldi, “*Glueball masses in the large N limit*”, JHEP **1008**, 119 (2010) [arXiv:1007.3879 [hep-lat]].
- [23] G. S. Bali *et al.* [TXL and T(X)L Collaborations], “*Static potentials and glueball masses from QCD simulations with Wilson sea quarks*”, Phys. Rev. D **62**, 054503 (2000) [hep-lat/0003012]. C. McNeile *et al.* [UKQCD Collaboration], “*Mixing of scalar glueballs and flavor singlet scalar mesons*”, Phys. Rev. D **63**, 114503 (2001) [hep-lat/0010019]. A. Hart *et al.* [UKQCD Collaboration], “*On the glueball spectrum in $O(a)$ improved lattice QCD*”, Phys. Rev. D **65**, 034502 (2002) [hep-lat/0108022], “*A Lattice study of the masses of singlet 0^{++} mesons*”, Phys. Rev. D **74**, 114504 (2006) [hep-lat/0608026].
- [24] S. Narison, “*Spectral Function Sum Rules for Gluonic Currents*”, Z. Phys. **C26** (1984) 209; “*QCD tests of the puzzling scalar mesons*”, Phys. Rev. **D73** (2006) 114024; “*Masses, decays and mixings of gluonia in QCD*”, Nucl. Phys. **B509** (1998) 312.
- [25] S. S. Gubser, A. Nellore, S. S. Pufu and F. D. Rocha, “*Thermodynamics and bulk viscosity of approximate black hole duals to finite temperature quantum chromodynamics*”, Phys. Rev. Lett. **101**, 131601 (2008) [arXiv:0804.1950 [hep-th]].

- [26] S. Narison and G. Veneziano, “*QCD Tests of $G(1.6)=\text{Glueball}$* ”, Int. J. Mod. Phys. **A4** (1989) 2751.
- [27] C. Csaki and M. Reece, “*Toward a systematic holographic QCD: A Braneless approach*”, JHEP **0705** (2007) 062 [arXiv:hep-ph/0608266].
- [28] B. Batell and T. Gherghetta, “*Dynamical Soft-Wall AdS/QCD*”, Phys. Rev. **D78** (2008) 026002 [arXiv:hep-ph/0801.4383]. W. de Paula, T. Frederico, H. Forkel, M. Beyer, “*Dynamical holographic QCD with area-law confinement and linear Regge trajectories*”, Phys. Rev. **D79** (2009) 075019 [arXiv:hep-ph/0806.3830v2].
- [29] F. Jugeau, S. Narison and H. Ratsimbarison, “*SVZ+1/q² expansion versus some QCD holographic models of*” [arXiv:hep-ph/1302.6909].
- [30] L. Susskind and E. Witten, “*The Holographic bound in anti-de Sitter space*”, hep-th/9805114.
- [31] D.-F. Zeng, “*Heavy quark potentials in some renormalization group revised AdS/QCD models*”, Phys. Rev. D **78**, 126006 (2008) [arXiv:0805.2733 [hep-th]].
- [32] J. Alanen and K. Kajantie, “*Thermodynamics of a field theory with infrared fixed point from gauge/gravity duality*”, Phys. Rev. D **81**, 046003 (2010) [arXiv:0912.4128 [hep-ph]].
- [33] T. A. Ryttov and F. Sannino, “*Supersymmetry inspired QCD beta function*”, Phys. Rev. D **78**, 065001 (2008) [arXiv:0711.3745 [hep-th]].
- [34] S. Bethke, “*The 2009 World Average of α_s* ”, Eur. Phys. J. C **64**, 689 (2009) [arXiv:0908.1135 [hep-ph]].
- [35] G. F. de Teramond and S.J. Brodsky *et al.*, “*Light-Front Holography and Gauge/String Duality: The Light Meson and Baryon Spectra*”, Nucl. Phys. Proc. Suppl. **199** (2012) 89 [hep-ph/0909.3900]; F. Zuo, “*Improved Soft-wall model with a negative dilaton*”, Phys. Rev. D **82** (2010) 086011 [hep-ph/0909.4240].
- [36] A. Karch *et al.*, “*On the sign of the dilaton in the soft-wall models*”, JHEP 1104 (2011) 066 [hep-ph/1012.4813]; S.J. Brodsky *et al.*, “*Nonperturbative QCD coupling and its β -function from Light-Front Holography*”, Phys. Rev. D **81** (2010) 096010 [hep-ph/1002.3948]; S. Nicotri, “*Phenomenology of The Holographic Soft-Wall Model of QCD With ”Reversed” Dilaton*”, AIP Conf. Proc. **1317** (2011) 322 [hep-ph/1009.4829]; T. Gutsche *et al.*, “*Dilaton in a Soft Wall holographic approach to mesons and baryons*”, Phys. Rev. D **85** (2012) 076003 [hep-ph/1108.0346]; S.S. Afonin, “*Soft Wall model with inverse exponential profile as a model for the axial and pseudoscalar mesons*”, Int. J. Mod. Phys. **A27** (2012) 1250171 [hep-ph/1207.2644]; G. F. de Teramond, H. G. Dosh and S. J. Brodsky, “*Kinematical and Dynamical Aspects of Higher-Spin Bound-State Equations in Holographic QCD*” [hep-ph/1301.1651].